Hindawi
Heteroatom Chemistry
Volume 2020, Article ID 9483520, 13 pages
https://doi.org/10.1155/2020/9483520

*Research Article*

# Efficient $ZrO(NO_3)_2.2H_2O$ Catalyzed Synthesis of 1*H*-Indazolo [1,2-*b*] phthalazine-1,6,11(13*H*)-triones and Electronic Properties Analyses, Vibrational Frequencies, NMR Chemical Shift Analysis, MEP: A DFT Study

**Forozan Piryaei, Nahid Shajari, and Hooriye Yahyaei**

*Department of Chemistry, Zanjan Branch, Islamic Azad University, P.O. Box 49195-467, Zanjan, Iran*

Correspondence should be addressed to Nahid Shajari; shajari_nahid@yahoo.com

Received 17 August 2019; Revised 26 October 2019; Accepted 11 November 2019; Published 1 March 2020

Academic Editor: Xing-Hai Liu



The synthesis of 1*H*-indazolo[1,2-*b*]phthalazine-1,6,11(13*H*)-trione derivatives, using one-pot three-component condensation reaction of 3-nitrophthalic anhydride, hydrazine monohydrate, dimedone, and aromatic aldehydes in the presence of $ZrO(NO_3)_2.2H_2O$ as the novel catalyst and in reflux conditions in EtOH was reported. Quantum theoretical calculations for three structures of compounds (**5a**, **5b**, and **5c**) were performed using the Hartree–Fock (HF) and density functional theory (DFT). From the optimized structure, geometric parameters were obtained and experimental measurements were compared with the calculated data. The structures of the products were confirmed by IR, $^1$H NMR, $^{13}$C NMR, mass spectra, and elemental analyses. The IR spectra data and $^1$H NMR and $^{13}$C NMR chemical shift computations of the 1*H*-indazolo[1,2-*b*]phthalazine-1,6,11(13*H*)-trione derivatives in the ground state were calculated. Frontier molecular orbitals (FMOs), total density of states (DOS), thermodynamic parameters, and molecular electrostatic potential (MEP) of the title compounds were investigated by theoretical calculations. Molecular properties such as the ionization potential (I), electron affinity (A), chemical hardness ($\eta$), electronic chemical potential ($\mu$), and electrophilicity ($\omega$) were investigated for the structures. Thus, there was an excellent agreement between experimental and theoretical results.

## 1. Introduction

The nitrogen-containing heterocyclic compounds are extensive in nature and play a unique role in biological systems [1–3]. Heterocycles containing the phthalazine ring are important compounds with broad biological activities, such as anticonvulsant [4], vasorelaxant [5], cardiotonic [6], cytotoxic [7], antimicrobial [8], anticonvulsant [9], antifungal [10], anticancer [11], and anti-inflammatory [12]. Several methods have been reported in the literature for the synthesis of 1*H*-indazolo[1,2-*b*]phthalazine-1,6,11(13*H*)-trione derivatives which have been reported using $Mg(HSO_4)_2$ [13], [Bmim]Br [14], *p*-TSA [15], silica sulfuric acid [16], PPA–$SiO_2$ [17], $H_2SO_4/H_2O$–EtOH and $H_2SO_4$/[bmim]$BF_4$ [18], $Ce(SO_4)_2.4H_2O$ [19], and starch sulfate [20], as catalysts. Given the interest in the synthesis of heterocycles [21–24], we described herein a simple synthesis of 1*H*-indazolo[1, 2-*b*]phthalazinetriones by three-component condensation reaction of phthalhydrazide, dimedone, and aromatic aldehydes in the presence of a catalytic amount of $ZrO(NO_3)_2.2H_2O$ at reflux conditions in EtOH. In recent years, computational chemistry has become an important tool for chemists and a well-accepted partner for experimental chemistry [25]. Computational chemistry is the application of computer simulation to predict or interpret chemical reactivity. Computational organic chemistry is an important area within which occur the determination of the mechanisms of chemical reactions [26, 27] especially catalysis [28, 29]structural determination of organic compounds [30, 31] prediction of spectroscopic data such as $^1$H NMR and $^{13}$C NMR chemical shifts [32, 33] properties calculation of organic molecules [34, 35] and the interaction

of a substrate with an enzyme [36]. This study has revealed some potential leads for possible pharmaceutical applications, and further research may help in the development of new antioxidative agents for important metabolic functions. Also, three new crystal structures of the compounds **5a**, **5b,** and **5c** are reported. In the present work, we investigated the energetic and structural properties of three compounds of 1*H*-indazolo[1,2-*b*]phthalazine-1,6,11(13*H*)-trione derivatives (**5a**, **5b,** and **5c**), using the DFT calculations. The optimized geometries, quantum molecular descriptors, IR spectra data, $^1$H NMR and $^{13}$C NMR chemical shift computations, molecular electrostatic potential (MEP), thermodynamic and electronic properties, and NBO analysis were calculated through density functional theory (DFT) and Hartree–Fock (HF) methods.

## 2. Materials and Methods

The starting materials and solvents were obtained from Merck (Germany) and Fluka (Switzerland) and were used without further purification. The melting points were measured with an Electrothermal 9100 apparatus and were uncorrected. The IR spectra were recorded on a Jasco FT-IR 6300 spectrometer. The $^1$H NMR and $^{13}$C NMR spectra were measured ($CDCl_3$ solution) with a Bruker DRX-250 Avance spectrometer at 250.0 and 62.9 MHz, respectively. Mass spectra were recorded with an Agilent Technologies 5975°C mass spectrometer. The elemental analyses were carried out using a Heraeus CHN-O-rapid analyzer.

*2.1. General Procedure for the Synthesis of $^1$H-indazolo[1,2-b] phthalazine-1,6,11(13H)-triones.* 3-Nitrophthalic anhydride (**1**, 1 mmol) and hydrazine monohydrate (**2**, 1 mmol)) were refluxed in ethanol for 15 minutes to form phthalhydrazide as an intermediate. Then, we added dimedone (**3**, 1 mmol) and aromatic aldehydes (**4**, 1 mmol) to the mixture of this reaction one by one in the presence of $ZrO(NO_3)_2.2H_2O$ (2 mol%) and the mixture was refluxed again for 2-3 hours. The completion of the reaction was checked by TLC. The solvent was removed under reduced pressure, and the viscous residue was purified by a preparative layer chromatography (silica gel; petroleum ether–ethyl acetate (8 : 2)). The solvent was removed under a reduced pressure and the products **5a**–**c** were obtained.

*2.2. Computational Studies.* In the present study, we carried out quantum theoretical calculations for the compounds **5a**, **5b**, and **5c** using the HF/6-31+G*, HF/6–311+G**, B3LYP/6-31+G*, and B3LYP/6–311+G** levels [37] by the Gaussian 03W program package [38] and calculated their properties. During the beginning stage, we obtained an optimized structure using Gaussian 03W program (see Figure 1). Then, we calculated the $^1$H NMR chemical shifts using the HF/6-31+G*, HF/6–311+G**, B3LYP/6-31+G*, and B3LYP/6–311+G** levels for the title compounds (**5a**, **5b,** and **5c**) and $^{13}$C NMR [39]. The electronic properties included energy of the highest occupied molecular orbital (EHOMO), energy of the lowest unoccupied molecular orbital (ELUMO), HOMO-LUMO energy gap ($\Delta E$), ELUMO, natural charges, and molecular properties [40]. The optimized molecular structure, HOMO and LUMO surfaces were visualized using GaussView 03 program [41].

## 3. Results and Discussion

The three-component reaction between 3-nitro phthalhydrazide **(6)**, dimedone **(3)**, and aromatic aldehydes **(4)** proceeded very smoothly and cleanly in the presence of a catalytic amount of $ZrO(NO_3)_2.2H_2O$ at reflux conditions in ethanol and afforded the corresponding 1*H*-indazolo[1,2-*b*]phthalazine-1,6,11(13*H*)-trione derivatives **(5a-c)** in high yields (Scheme 1 and Table 1), and no undesirable side reactions were observed. A mechanistic rationalization for this reaction is provided in Scheme 2. The structures of the products were deduced from their IR, $^1$H NMR, $^{13}$C NMR, mass spectra and elemental analyses. For example, the $^1$H NMR spectrum of **5a** exhibited distinct signals arising from two $CH_3$ groups of dimedone (0.96 and 1.00 ppm, 2 s), two $CH_2$ groups of dimedone ring (2.07–2.33 ppm, m) and (3.65 ppm, s), one $OCH_3$ group of 4-methoxyphenyl ring (3.80 ppm, s), aliphatic CH (5.25 ppm, s), and seven aromatic CH (7.02 ppm, d, $^3J_{HH}$ = 8.25 Hz), (7.78 ppm, d, $^3J_{HH}$ = 8.25 Hz), and (8.50–8.82, m). The $^{13}$C NMR spectrum of **5a** shows 22 distinct resonances arising from two $CH_3$ groups (26.91 and 28.16 ppm), C (32.24 ppm), two $CH_2$ groups (42.49 and 50.74 ppm), $OCH_3$ (55.81 ppm), aliphatic CH (64.46 ppm), aromatic and olefinic carbons (113.66, 114.83, 127.03, 127.99, 128.71, 129.08, 129.41, 129.96, 130.40, 131.97, 135.29, and 136.87 ppm), and C=O carbons (160.84, 162.12, and 196.47 ppm). The mass spectrum of **5a** displays a molecular ion peak at m/z 447.

*3.1. Characterization Data for the Synthesis of 1H-indazolo [1,2-b]phthalazine-1,6,11(13H)-trione Derivatives **(5a-c)***

*3.1.1. 3,3-Dimethyl-13-(4-methoxyphenyl)-10-nitro-2,3,4,13-tetrahydro-1H-indazolo[1,2-b] phthalazine-1,6,11(13H)-trione **(5a)**.* Yellow solid; m.p.>250°C; Yield: 75%; Anal. Calcd for $C_{24}H_{21}N_3O_6$ (447.4): C, 64.42; H, 4.73; N, 9.39 %. Found: C, 64.38; H, 4.75; N, 9.33; IR (KBr) ($\upsilon_{max}$, $cm^{-1}$): 3439, 2959, 1728 (C=O), 1666 (C=O), 1602 (C=O), 1535 ($NO_2$-Asymmetric Str.), 1464, 1358 ($NO_2$-Symmetric Str.); $^1$H NMR (DMSO. $d_6$, 250.0 MHz): $\delta_H$ 0.96 (3H, *s*, $CH_3$), 1.00 (3H, *s*, $CH_3$), 2.07–2.33 (2H, *m*, $CH_2$), 3.65 (2H, *s*, $CH_2$), 3.80 (3H, *s*, $OCH_3$), 5.25 (1H, *s*, CH), 7.02 (2H, *d*, $^3J_{HH}$ = 8.25 HZ, arom CH), 7.78 (2H, *d*, $^3J_{HH}$ = 8.25 HZ, arom CH), 8.50–8.82 (3H, *m*, arom CH); $^{13}$C NMR (DMSO. $d_6$, 62.9 MHz): $\delta_C$ 26.91 and 28.16 ($2CH_3$), 32.24 (C), 42.49 ($CH_2$), 50.74 ($CH_2$), 55.81 ($OCH_3$), 64.46 (CH), 113.66, 114.83, 127.03, 127.99, 128.71, 129.08, 129.41, 129.96, 130.40, 131.97, 135.29, and 136.87 (aromatic and olefinic carbons), 160.84, 162.12, and 196.47 (3C=O); MS (EI): *m/z* 447 ($M^+$, 0.02), 286 (5), 269 (100), 253 (9), 241 (27), 161 (76), 134 (27), 91 (24), 77 (33), and 63 (13).

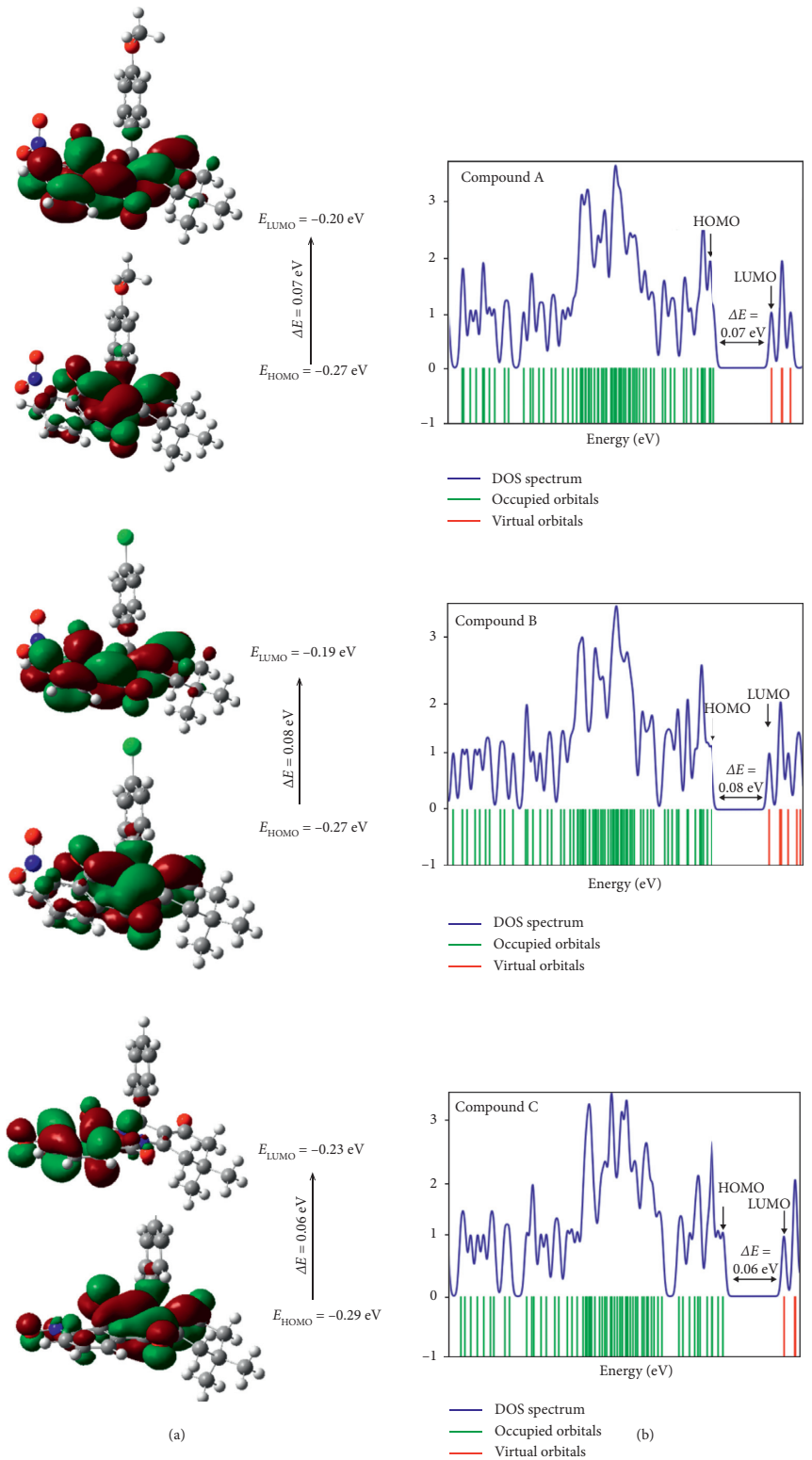


FIGURE 1: (a) Calculated frontier molecular orbitals of compounds **5a**, **5b,** and **5c** (ΔE: energy gap between LUMO and HOMO). (b) Calculated DOS plots of the title compounds (using B3LYP/6-311+G(d)).

*3.1.2. 3,3-Dimethyl-10-nitro-13-phenyl-2,3,4,13-tetrahydro-1H-indazolo[1,2-b]phthalazine-1,6,11(13H)-trione* ***(5b).*** Yellow solid; m.p.>250°C; Yield: 80%; Anal. Calcd for $C_{23}H_{19}N_3O_5$ (417.4): C, 66.18; H, 4.59; N, 10.07 %. Found: C, 66.25; H, 4.54; N, 10.00; IR (KBr) ($\upsilon_{max}$, $cm^{-1}$): 2931, 2358, 1724 (C=O), 1617 (C=O), 1588 (C=O), 1539 ($NO_2$-Asymmetric Str.), 1460, 1410 ($NO_2$ - Symmetric Str.); $^1H$ NMR (DMSO. $d_6$, 250.0 MHz): $\delta_H$ 0.96 (3H, *s*, $CH_3$), 1.24 (3H, *s*,

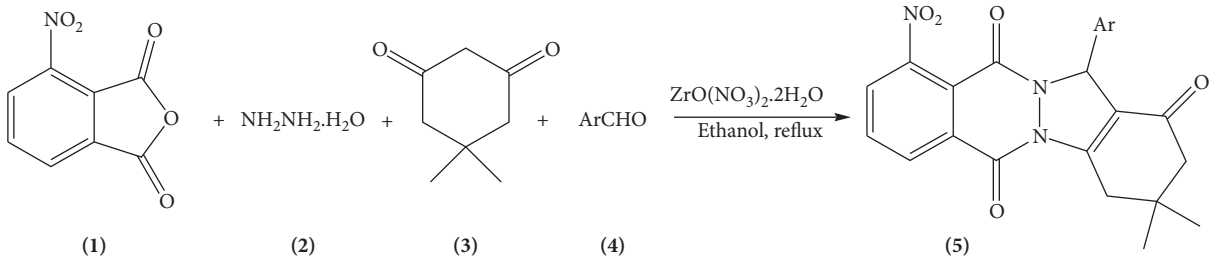


Scheme 1: Three-component reaction of 3-nitrophthalic anhydride, hydrazine monohydrate, dimedone, and aromatic aldehydes (see Table 1).

Table 1: Synthesis of 1*H*-indazolo[1,2-*b*]phthalazine-1,6,11(13*H*)-trione derivatives **(5a-c)**.

| **5** | Ar | % Yield |
|---|---|---|
| **a** | 4-Methoxyphenyl | 75 |
| **b** | Phenyl group | 80 |
| **c** | 4-Chlorophenyl group | 78 |

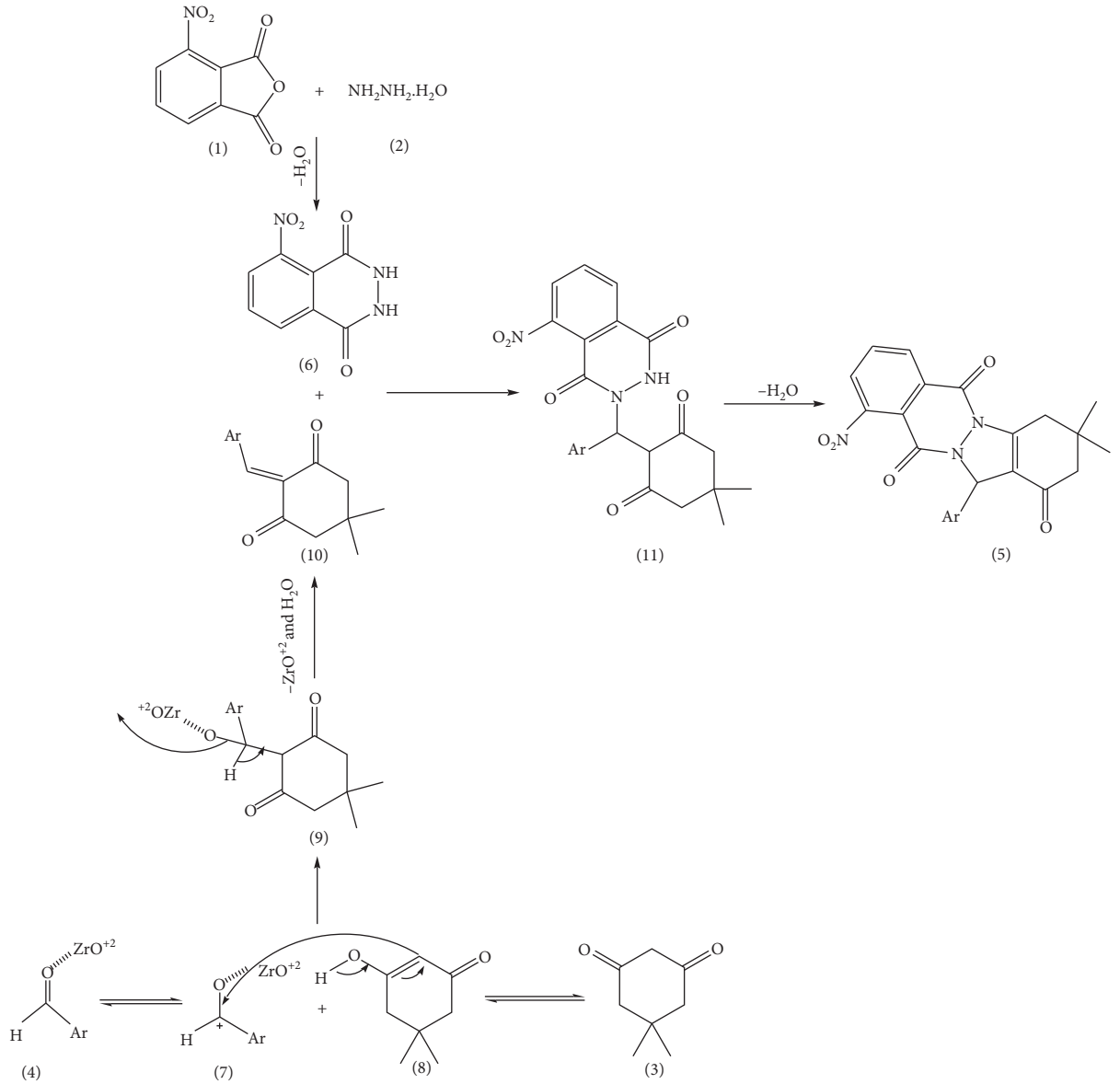


Scheme 2: A proposed mechanism for the formulation of 1*H*-indazolo[1,2-*b*]phthalazine-1,6,11(13*H*)-trione derivatives **(5a-c)**.

$CH_3$), 2.07–2.23 (2H, *m*, $CH_2$), 3.87–3.92 (2H, *m*, $CH_2$), 5.26 (1H, *s*, CH), 7.36–8.69 (9H, *m*, arom CH); $^{13}$C NMR (DMSO. $d_6$, 62.9 MHz): $\delta_C$ 28.15 and 28.50 ($2CH_3$), 32.47 (C), 42.49 ($CH_2$), 50.74 ($CH_2$), 64.44 (CH), 126.81, 128.29, 128.44, 128.56, 128.79, 129.14, 129.32, 130.78, 131.76, 131.95, 134.25, and 135.31 (aromatic and olefinic carbons), 161.82, 165.50, and 198.19 (3C=O).

*3.1.3. 13-(4-Chlorophenyl)-3,3-dimethyl-10-nitro-2,3,4,13-tetrahydro-1H-indazolo[1,2-b]phthalazine-1,6,11(13H)-trione **(5c)**.* Yellow Solid; m.p. >250°C; Yield: 78%; Anal. Calcd for $C_{23}H_{18}ClN_3O_5$ (451.9): C, 61.14; H, 4.02; N, 9.30 %. Found: C, 61.10; H, 4.04; N, 9.24; IR (KBr) ($\upsilon_{max}$, $cm^{-1}$): 2928, 2358, 1728 (C=O), 1611 (C=O), 1591 (C=O), 1474 ($NO_2$- Asymmetric Str.), 1393 ($NO_2$-Symmetric Str.), 1085 (C–Cl); $^1$H NMR (DMSO. $d_6$, 250.0 MHz): $\delta_H$ 0.94 (3H, *s*, $CH_3$), 1.22 (3H, *s*, $CH_3$), 2.05–2.20 (2H, *m*, $CH_2$), 3.87 (2H, *s*, $CH_2$), 5.23 (1H, *s*, CH), 7.15–8.66 (8H, *m*, arom CH); $^{13}$C NMR (DMSO. $d_6$, 62.9 MHz): $\delta_C$ 26.82 and 28.12 ($2CH_3$), 32.45(C), 42.43 ($CH_2$), 50.68 ($CH_2$), 64.45 (CH), 114.38, 123.32, 128.22, 128.67, 128.90, 129.07, 129.26, 129.46, 129.89, 130.34, 133.01, and 134.70 (aromatic and olefinic carbons), 161.00, 163.41, and 196.43 (3C=O).

### 3.2. Computational Section

*3.2.1. IR Spectroscopy.* Harmonic vibrational frequencies of the title compounds were calculated using the B3LYP/3-21G, HF/3-21G, B3LYP/6-311+G(d), and HF/6-311+G(d) levels. The vibrational frequencies assignments were made using the GaussView program. Some of the characteristic frequencies are provided in Tables 2–4. The harmonic frequencies calculated by DFT are usually higher than the corresponding experimental values due to the approximate treatment of the electron correlation, anharmonicity effects, and basis set deficiencies [39].

For the title compound **(5a)**, the strong band at 3376 $cm^{-1}$ in the FT-IR spectrum is assigned as $\nu_{C=O}$ mode. The calculated values for this mode are 3375, 3204, 3227, and 3360 $cm^{-1}$ for HF/6-31+G*, HF/6–311+G**, B3LYP/6-31+G*, and B3LYP/6–311+G** levels, respectively. For the title compound **(5a)**, the strong band at 3439, 2959, and 1728 $cm^{-1}$ in the FT-IR spectrum is assigned as $\nu_{C=O}$ mode. The calculated values for this mode are the same as those calculated for HF/3-21G, HF/6-311+G**, B3LYP/3-21G, and B3LYP/6-311+G** levels, respectively. The DFT computation predicts this vibrational mode in ArC=C at 1464 $cm^{-1}$ for A, 1489 $cm^{-1}$ for the compound **5b,** and 1493 $cm^{-1}$ for the compound **5c**. This observed frequency coincides well with the expected value [42]. There was an excellent agreement between experimental and theoretical results for all used methods. In order to compare this agreement, the correlation graphic based on the theoretical and experimental data was investigated. A small difference between the experimental and calculated vibrational modes was observed. This difference might have been due to intermolecular hydrogen bonding formation. Also, the experimental results belong to the solid phase while theoretical calculations belong to the isolated gaseous phase.

*3.2.2. NMR Parameters.* The calculation of $^1$H NMR and $^{13}$C NMR chemical shifts of compounds 5a, 5b, and 5c is done at B3LYP/3-21G, HF/3-21G, B3LYP/6-311+G(d), and HF/6-311+G(d) levels. The experimental and calculated $^1$H NMR and $^{13}$C NMR chemical shifts of 1*H*-indazolo[1,2-*b*] phthalazine-1,6,11(13*H*)-trione derivatives (**5a**, **5b** and **5c**) are presented in Tables 5–10. Based on our calculations and experimental spectra, we made a reliable one-to-one correspondence between our fundamentals, and all of the chemical shifts were calculated by the HF and B3LYP methods. For the title compound **(5a)**, the aromatic CH protons appeared at $\delta_H$ 7.02–8.82 ppm, and the calculated amounts at HF/6-311+G** and B3LYP/6-311+G** basis set levels were at 7.30–8.19 and 7.00–8.89 ppm, respectively. Protons of two methyl groups appeared at $\delta_H$ 0.96 and 1.00 ppm, the calculated amounts at HF/6-311+G** and B3LYP/6-311+G** basis set levels were at 0.67 and 1.28 ppm and 0.86 and 1.19 ppm, respectively. Also, chemical shifts of three carbonyl groups appeared at $\delta_c$ 160.84, 162.12, and 196.47 ppm, the calculated amounts at HF/6-311+G** and B3LYP/6-311+G** basis set levels were at 149.88, 153.99, and 190.97 ppm and 159.51, 161.27, and 197.32 ppm, respectively. The same was true for other compounds.

There was an excellent agreement between experimental and theoretical results for all methods employed. In order to compare this agreement, the correlation graphic based on the theoretical and experimental data was investigated. The correlation value ($R^2$) for compounds at HF/3-21G, B3LYP/3-21G**,** HF/6-311+G**, and B3LYP/6-311+G** is presented in Table 11. There was an excellent agreement between experimental and theoretical results [39]. A small difference between the experimental and calculated vibrational modes was observed. This difference might have been due to the intermolecular hydrogen bonding formation. Furthermore, the experimental results belong to the solid phase while and theoretical calculations belong to the isolated gaseous phase.

*3.2.3. Electronic Properties.* Quantum chemical methods are important for obtaining information about molecular structure and electrochemical behavior. A frontier molecular orbital (FMO) analysis was performed for the compounds using the B3LYP/6-311+G(d) level [38]. FMO results such as EHOMO, ELUMO, and the HOMO-LUMO energy gap ($\Delta E$) of the title compounds are summarized in Table 7. The energy of the LUMO, HOMO, and their energy gaps reflected the chemical reactivity of the molecule [43]. In addition, the HOMO could act as an electron donor and the LUMO as an electron acceptor. A higher HOMO energy (EHOMO) for the molecule indicated a higher electron-donating ability to an appropriate acceptor molecule with a low-energy empty molecular orbital [44]. As shown in Figure 1 the HOMO energy of the compound **5c** had the highest value (−0.29 eV). A large energy gap implied high stability for the molecule. The calculated values of the

Table 2: The selected experimental and theoretical frequencies of the title compounds using the B3LYP and HF methods for compound **(5a)**.

| Experimental wavenumbers by FT-IR ($cm^{-1}$) | | | Calculated vibrational wavenumbers by HF and DFT methods ($cm^{-1}$) | | | |
|---|---|---|---|---|---|---|
| | | | B3LYP | | HF | |
| | | | 3-21G | 6-311+G** | 3-21G | 6-311+G** |
| Assignment | | 3439 | 3441 | 3440 | 3438 | 3450 |
| | C=O | 2959 | 2967 | 2955 | 2964 | 2960 |
| | | 1728 | 1721 | 1729 | 1720 | 1733 |
| | C=O | 1666 | 1691 | 1673 | 1689 | 1682 |
| | C=O | 1602 | 1602 | 1608 | 1615 | 1600 |
| | C=C | 1535 | 1599 | 1530 | 1542 | 1535 |
| | Ar C=C | 1464 | 1466 | 1466 | 1463 | 1469 |
| | $CH_3$ | 1358 | 1351 | 1359 | 1368 | 1366 |

Table 3: The selected experimental and theoretical frequencies of the title compounds using the B3LYP and HF methods for compound **(5b)**.

| Experimental wavenumbers by FT-IR ($cm^{-1}$) | | | Calculated vibrational wavenumbers by HF and DFT methods ($cm^{-1}$) | | | |
|---|---|---|---|---|---|---|
| | | | B3LYP | | HF | |
| | | | 3-21G | 6-311+G** | 3-21G | 6-311+G** |
| Assignment | | 3413 | 3413 | 3405 | 3461 | 3423 |
| | C=O | 2955 | 2972 | 2915 | 2952 | 2962 |
| | | 1661 | 1660 | 1663 | 1668 | 1671 |
| | C=O | 1626 | 1619 | 1628 | 1630 | 1629 |
| | C=H | 1583 | 1573 | 1588 | 1589 | 1573 |
| | Ar C=C | 1489 | 1489 | 1490 | 1498 | 1499 |
| | $CH_3$ | 1362 | 1397 | 1362 | 1373 | 1307 |
| | C–Cl, bending | 1090 | 1080 | 1090 | 1099 | 1088 |

Table 4: The selected experimental and theoretical frequencies of the title compounds using the B3LYP and HF methods for compound **(5c)**.

| Experimental wavenumbers by FT-IR ($cm^{-1}$) | | | Calculated vibrational wavenumbers by HF and DFT methods ($cm^{-1}$) | | | |
|---|---|---|---|---|---|---|
| | | | B3LYP | | HF | |
| | | | 3-21G | 6-311+G** | 3-21G | 6-311+G** |
| Assignment | | 3436 | 3430 | 3430 | 3449 | 3435 |
| | C=O | 2951 | 2971 | 2962 | 2973 | 2943 |
| | | 1661 | 1669 | 1661 | 1750 | 1665 |
| | C=O | 1625 | 1638 | 1640 | 1615 | 1635 |
| | C=C | 1576 | 1583 | 1579 | 1580 | 1579 |
| | Ar C=C | 1492 | 1483 | 1492 | 1489 | 1497 |
| | $CH_3$ | 1361 | 1361 | 1361 | 1373 | 1360 |

Table 5: Experimentally measured and calculated $^1$H chemical shifts $\delta$ (ppm vs TMS) of the compound **(5a)**.

| $^1$H NMR | EXP | Calculated | | | |
|---|---|---|---|---|---|
| | | B3LYP/3-21G | B3LYP/6-311+G** | HF/3-21G | HF/6-311+G** |
| **3H, s, $CH_3$** | **0.96** | 0.33 | 0.86 | 0.66 | 0.67 |
| **3H, s, $CH_3$** | **1.00** | 1.41 | 1.19 | 1.15 | 1.28 |
| **2H, m, $CH_2$** | **2.07–2.33** | 2.38–2.52 | 2.03–2.33 | 1.95–2.60 | 1.95–2.60 |
| **2H, s, $CH_2$** | **3.65** | 3.32 | 3.60 | 3.13 | 3.13 |
| **3H, s, $OCH_3$** | **3.80** | 3.78 | 3.88 | 3.66 | 3.66 |
| **1H, s, CH** | **5.25** | 5.25 | 5.50 | 5.81 | 5.81 |
| **2H, d, arom C–H** | **7.02** | 7.02 | 7.00 | 7.30 | 7.30 |
| **2H, d, arom C–H** | **7.78** | 7.11 | 7.70 | 7.44 | 7.44 |
| **4H, m, arom C–H** | **8.50–8.82** | 8.22–8.75 | 8.51–8.89 | 8.08–8.17 | 8.08–8.19 |

HOMO-LUMO energy gap ($\Delta E$) for the structures **5a**, **5b,** and **5c** were 0.07, 0.08, and 0.06 eV, respectively. DOS plots [45] also demonstrated the calculated energy gaps ($\Delta E$) for the compounds **5a**, **5b,** and **5c** (see Figure 2). It is obvious that the energy gap of the compound **5b** was the highest (0.08 eV); therefore, it was less reactive than the other

Table 6: Experimentally measured and calculated $^{13}C$ chemical shifts $\delta$ (ppm vs TMS) of the compound **(5a)**.

| $^{13}C$ NMR | EXP | Calculated | | | |
|---|---|---|---|---|---|
| | | B3LYP/3-21G | B3LYP/6-311+G** | HF/3-21G | HF/6-311+G** |
| **$2CH_3$** | **26.91–28.16** | 26.26–27.78 | 26.90–27.99 | 18.82–30.50 | 26.80–27.01 |
| **C** | **32.24** | 31.10 | 31.99 | 32.62 | 30.37 |
| **$CH_2$** | **42.49** | 42.83 | 42.73 | 45.54 | 44.99 |
| **$CH_2$** | **50.74** | 49.01 | 49.41 | 46.01 | 46.89 |
| **CH** | **64.46** | 63.98 | 62.99 | 58.79 | 60.74 |
| **$OCH_3$** | **55.81** | 50.11 | 55.88 | 48.72 | 50.11 |
| **C-H aromatic and olefinic carbons** | **113.66** | 93.78 | 113.52 | 101.98 | 107.09 |
| | **114.83** | 94.99 | 113.99 | 108.88 | 111.90 |
| | **127.99** | 95.08 | 126.31 | 110.44 | 123.53 |
| | **128.71** | 95.39 | 130.07 | 111.47 | 123.43 |
| | **128.71** | 96.14 | 131.05 | 112.90 | 122.90 |
| | **129.08** | 96.87 | 130.66 | 113.02 | 125.51 |
| | **129.41** | 97.60 | 133.98 | 114.13 | 124.39 |
| | **129.96** | 97.65 | 136.75 | 114.48 | 124.19 |
| | **130.40** | 119.1 | 138.41 | 114.56 | 124.97 |
| | **131.97** | 122.79 | | 127.99 | 126.65 |
| | **135.29** | 127.76 | | 137.19 | 137.19 |
| | **136.87** | 129.30 | | 138.90 | 144.90 |
| **C=O(1)** | **160.84** | — | 159.51 | — | 149.88 |
| **C=O(2)** | **162.12** | — | 161.27 | — | 153.99 |
| **C=O(3)** | **196.47** | — | 197.32 | — | 190.97 |

Table 7: Experimentally measured and calculated $^{1}H$ chemical shifts $\delta$ (ppm vs TMS) of the compound **(5b)**.

| $^{1}H$ NMR | EXP | Calculated | | | |
|---|---|---|---|---|---|
| | | B3LYP/3-21G | B3LYP/6-311+G** | HF/3-21G | HF/6-311+G** |
| **3H, s, $CH_3$** | **0.94** | 0.43 | 0.98 | 0.48 | 0.97 |
| **3H, s, $CH_3$** | **1.22** | 1.42 | 1.27 | 1.30 | 1.30 |
| **2H, m, $CH_2$** | **2.05–2.20** | 2.11–2.32 | 2.08–2.28 | 2.17–2.96 | 2.09–2.48 |
| **2H, s, $CH_2$** | **3.87** | 3.94 | 3.90 | 4.00 | 3.98 |
| **1H, s, C–H** | **5.23** | 5.63 | 5.32 | 5.85 | 5.42 |
| **8H, m, arom C–H** | **7.15–8.66** | 7.10–7.97 | 7.17–8.62 | 7.19–8.91 | 7.19–8.76 |

Table 8: Experimentally measured and calculated $^{13}C$ chemical shifts $\delta$ (ppm vs TMS) of the compound **(5b)**.

| $^{13}C$ NMR | EXP | Calculated | | | |
|---|---|---|---|---|---|
| | | B3LYP/3-21G | B3LYP/6-311+G** | HF/3-21G | HF/6-311+G** |
| **$2CH_3$** | **26.82–28.12** | 26.43–29.11 | 26.83–29.11 | 25.31–31.74 | 28.88–30.11 |
| **C** | **32.45** | 37.41 | 32.51 | 36.42 | 36.77 |
| **$CH_2$** | **42.43** | 43.33 | 42.51 | 41.23 | 42.21 |
| **$CH_2$** | **50.68** | 58.13 | 51.67 | 59.11 | 57.32 |
| **CH** | **64.45** | 70.41 | 63.78 | 72.31 | 71.20 |
| **Aromatic and olefinic carbons** | **114.38** | 86.90 | 115.77 | 89.99 | 85.90 |
| | **123.32** | 93.88 | 123.46 | 97.67 | 91.63 |
| | **128.22** | 94.84 | 129.22 | 97.91 | 96.41 |
| | **128.67** | 97.22 | 129.63 | 83.23 | 126.99 |
| | **128.90** | 97.71 | 129.77 | 84.89 | 128.71 |
| | **129.07** | 97.97 | 130.11 | 85.99 | 128.86 |
| | **129.26** | 100.82 | 130.28 | 112.92 | 128.32 |
| | **129.46** | 101.89 | 130.49 | 113.55 | 129.27 |
| | **129.89** | 119.29 | 130.80 | 114.41 | 129.64 |
| | **130.34** | 127.48 | 131.45 | 129.99 | 129.83 |
| | **133.01** | 129.17 | 134.89 | 130.89 | 130.22 |
| | **134.70** | 148.29 | 135.03 | 137.98 | 134.60 |
| **C=O(1)** | **161.00** | — | 160.27 | — | 159.21 |
| **C=O(2)** | **163.41** | — | 162.11 | — | 160.41 |

Table 9: Experimentally measured and calculated $^{1}$H chemical shifts $\delta$ (ppm vs TMS) of the compound **(5c)**.

| $^{1}$H NMR | EXP | Calculated | | | |
|---|---|---|---|---|---|
| | | B3LYP/3-21G | B3LYP/6-311+G** | HF/3-21G | HF/6-311+G** |
| **3H, s, $CH_3$** | **0.96** | 0.53 | 0.97 | 0.69 | 0.78 |
| **3H, s, $CH_3$** | **1.24** | 1.40 | 1.29 | 1.84 | 1.48 |
| **2H, m, $CH_2$** | **2.07–2.23** | 1.83–2.32 | 2.11–2.29 | 1.95–2.10 | 1.96–2.11 |
| **2H, m, $CH_2$** | **3.87–3.92** | 2.86 | 3.80–3.94 | 3.10–3.51 | 3.18–3.68 |
| **1H, s, C-H** | **5.26** | 5.59 | 5.23 | 5.88 | 5.40 |
| **9H, m, arom C-H** | **7.36–8.69** | 7.06–7.19 | 7.33–8.68 | 7.18–8.16 | 7.11–8.39 |

Table 10: Experimentally measured and calculated $^{13}$C chemical shifts $\delta$ (ppm vs TMS) of the compound **(5c)**.

| $^{13}$C NMR | EXP | Calculated | | | |
|---|---|---|---|---|---|
| | | B3LYP/3-21G | B3LYP/6-311+G** | HF/3-21G | HF/6-311+G** |
| **$CH_3$** | **28.15** | 26.66 | 28.19 | 18.20 | 28.21 |
| **$CH_3$** | **28.50** | 28.19 | 28.93 | 18.70 | 28.87 |
| **C** | **32.47** | 30.11 | 33.11 | 30.65 | 32.76 |
| **$CH_2$** | **42.49** | 43.86 | 47.22 | 45.64 | 48.32 |
| **$CH_2$** | **50.74** | 50.11 | 50.66 | 48.11 | 50.98 |
| **CH** | **64.44** | 73.11 | 64.32 | 48.91 | 67.11 |
| **Aromatic and olefinic carbons** | **126.81** | 87.066 | 127.93 | 107.92 | 128.01 |
| | **128.29** | 92.77 | 129.48 | 108.21 | 128.32 |
| | **128.44** | 92.93 | 129.32 | 108.43 | 128.66 |
| | **128.67** | 93.60 | 129.51 | 108.74 | 128.51 |
| | **128.86** | 93.23 | 129.69 | 108.56 | 128.90 |
| | **129.14** | 96.53 | 130.11 | 109.85 | 133.66 |
| | **129.32** | 97.06 | 130.30 | 110.05 | 133.68 |
| | **130.78** | 97.73 | 130.79 | 110.48 | 133.99 |
| | **131.76** | 102.53 | 133.35 | 112.03 | 136.98 |
| | **131.95** | 119.2 | 133.78 | 113.08 | 136.31 |
| | **134.25** | 127.6 | 133.86 | 114.19 | 136.32 |
| | **135.31** | 129.46 | 139.21 | 118.79 | 137.38 |
| **C=O(1)** | **161.82** | — | 163.23 | 151.46 | 160.20 |
| **C=O(2)** | **165.50** | — | 169.93 | 153.24 | 161.39 |
| **C=O(3)** | **198.19** | — | 197.11 | 169.84 | 193.22 |

Table 11: Correlation of calculated and experimental $^{1}$H NMR,$^{13}$C NMR, and IR of the compounds.

| Compounds | | B3LYP/3-21G | B3LYP/6-311+G** | HF/3-21G | HF/6-311+G** |
|---|---|---|---|---|---|
| **5a** | **HNMR** | 0.9975 | 0.9999 | 0.9991 | 0.9974 |
| **5b** | | 0.9986 | 0.9999 | 0.9985 | 0.9997 |
| **5c** | | 0.9996 | 0.9995 | 0.9990 | 0.9998 |
| **5a** | **CNMR** | 0.9977 | 0.9995 | 0.9992 | 0.9975 |
| **5b** | | 0.9983 | 0.9999 | 0.9990 | 0.9998 |
| **5c** | | 0.9986 | 0.9998 | 0.9998 | 0.9999 |
| **5a** | **IR** | 0.9953 | 0.9995 | 0.9995 | 0.9978 |
| **5b** | | 0.9986 | 0.9999 | 0.9988 | 0.9990 |
| **5c** | | 0.9970 | 0.9997 | 0.9983 | 0.9991 |

structures, whereas the energy gap of the compound **5c** was the lowest (0.06 eV), which indicates that it was the most reactive. As presented in Figure 2, charge transfer could take place within the three molecules.

The electronic properties such as ionization potential, electron affinity, global hardness, electronic chemical potential, and electrophilicity are calculated in Table 12. The first ionization potential (I) and electron affinity (A) could be expressed through HOMO and LUMO orbital energies by connecting it with Hartree–Fock SCF theory and invoking Koopmans' theorem [46] as I = −EHOMO and A = −ELUMO. The chemical hardness ($\eta$ = I−A/2) is an important property that measures the molecular stability and reactivity [47]. A hard molecule has a large energy gap ($\Delta$E) and a soft molecule has a small energy gap ($\Delta$E) [48]. The chemical hardness ($\eta$) values of the compounds **5a**, **5b,** and **5c** were 0.170, 0.176, and 0.175 eV, respectively. Compound **5b** had the highest chemical hardness ($\eta$ = 0.176 eV); therefore, it was a hard

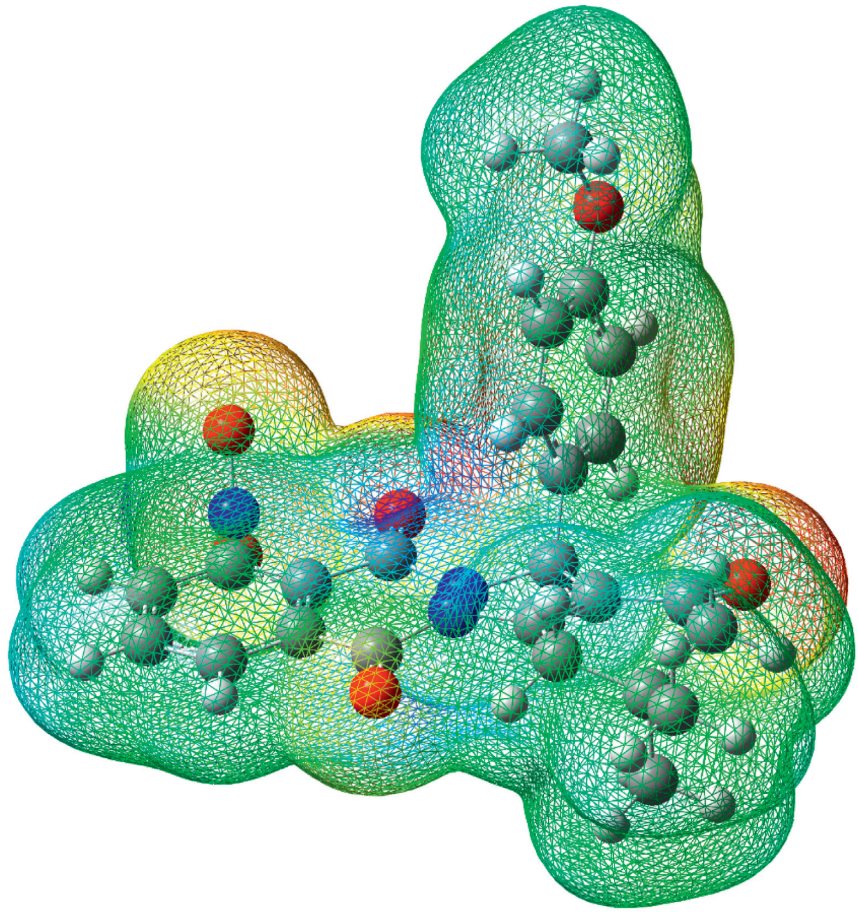

(a)

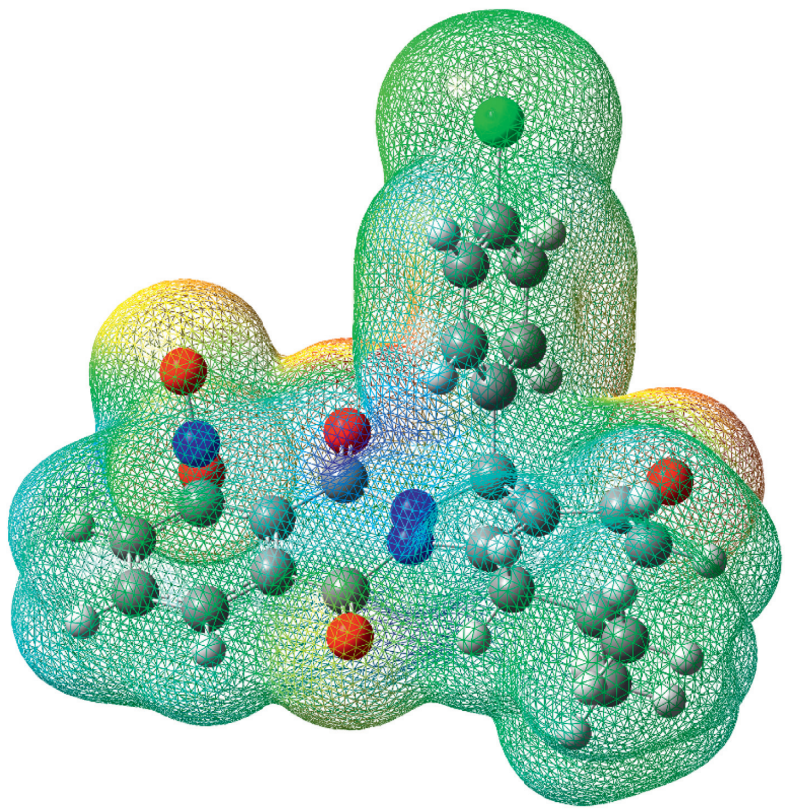

(b)

Figure 2: Continued.

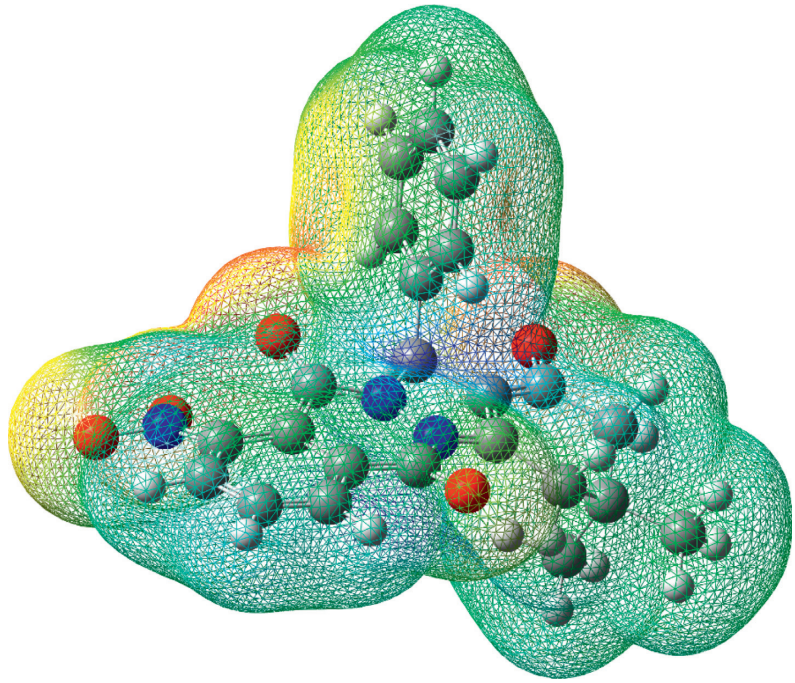

(c)

Figure 2: Molecular electrostatic potential (MEP) maps of the title compounds calculated using the B3LYP/6-311+G(d) level.

molecule with less reactivity and a high energy gap ($\Delta E = 0.08$ eV). The electronic chemical potential ($\mu = -(I + A)/2$) is a form of the potential energy that can be absorbed or released during a chemical reaction and that may also change during a phase transition [49]. The electronic chemical potential of **5c** had the most negative value (−0.26 eV). The electrophilicity (ω) measures the stabilization in energy when the system acquires an additional electronic charge from the environment. The electrophilicity index ($\omega = \mu 2/2\eta$) contains information about both electron transfer (chemical potential) and stability (hardness) and is a better descriptor of global chemical reactivity [50]. The higher value of electrophilicity index shows the high capacity of the molecule to accept electrons. The electrophilicity index for the compounds **5a**, **5b,** and **5c** was 0.0040, 0.0046, and 0.0059 eV, respectively. The compound **5c** had the highest electrophilicity index; therefore, it had a high capacity for accepting electrons. The dipole moment (μD) is a good measure of the asymmetric nature of a molecule. The size of the dipole moment depends on the composition and dimensionality of the 3D structures. As shown in Table 12, all structures had a high value of dipole moment and point group of C1, which reflected no symmetry in the structures. The dipole moment for the compound 5b (B3LYP/6-311+G(d) = 6.172 Debye) was higher than that for the compounds **5a** and **5c** (4.988 and 4.396 Debye, respectively).The high value for **5c** was due to its asymmetric character.

*3.2.4. Thermodynamic Analysis.* The total energy of a molecule consists of the sum of translational, rotational, vibrational, and electronic energies. The statistical thermochemical analysis of title compounds is carried out considering the molecule to be at room temperature of 25°C and 1 atmospheric pressure. The thermodynamic parameters such as zero-point vibrational energy, rotational constant, heat capacity (C), and the entropy (S) of the title compound by B3LYP/6-311+G(d) level are listed in Table 13. According to Table 13, the calculated values for compound **5a** and **5b** are larger than compound **5c**; therefore, compounds **5a** and **5b** have maximum stability compared to compound **5c** due to formation of intramolecular hydrogen bonding.

*3.2.5. Molecular Electrostatic Potential (MEP).* The molecular electrostatic potential (MEP) was calculated by the B3LYP/6-311+G (d) level. The MEP is related to the electronic density and is a very useful descriptor in understanding sites for electrophilic attack and nucleophilic reactions as well as hydrogen bonding interactions [45]. The negative regions (red color) of the MEP are related to electrophilic reactivity, and the positive (blue color) region is related to nucleophilic reactivity, as shown in Figure 2.

Molecular electrostatic potential (MEP) surface aims at locating the positive and negative charged electrostatic potential in the molecule. In each MEP surface, there is a color scale which indicates the negative and positive value. The red color is a sign for the negative extreme, and the blue color represents the positive extreme. The red color with a negative sign indicates the minimum electrostatic potential (which means it is bound loosely or has excess electrons), and it acts as electrophilic attack. The blue color also indicates the maximum of electrostatic potential, and it acts in the opposite manner.

Table 12: Absolute energy (a.u), dipole moment ($\mu$, Debye), frontier orbital energies (HOMO and LUMO, eV), hardness ($\eta$, eV), chemical potential ($\mu$, eV), and electrophilicity ($\omega$, eV) of **5a**, **5b**, and **5c** molecules.

| | $E_{HOMO}$ | $E_{LUMO}$ | $I$ | $A$ | $\mu$ | $\eta$ | $\omega$ | $\mu_D$ | Point group |
|---|---|---|---|---|---|---|---|---|---|
| **5a** | −0.27 | −0.20 | 0.27 | 0.20 | −0.235 | 0.170 | 0.0040 | 4.988 | C1 |
| **5b** | −0.27 | −0.19 | 0.27 | 0.19 | −0.230 | 0.176 | 0.0046 | 6.172 | C1 |
| **5c** | −0.29 | −0.23 | 0.29 | 0.23 | −0.260 | 0.175 | 0.0059 | 4.396 | C1 |

Table 13: Thermodynamic parameters of the **5a**, **5b**, and **5c** molecules using the B3LYP/6-311+G(d) level.

| | **5a** | **5b** | **5c** |
|---|---|---|---|
| Zero-point correction[a] | 0.439579 | 0.394413 | 0.405306 |
| Thermal correction to energy[b] | 0.468575 | 0.422073 | 0.431620 |
| Thermal correction to enthalpy[c] | 0.469519 | 0.423017 | 0.432564 |
| Thermal correction to Gibbs free energy[d] | 0.377501 | 0.333551 | 0.346912 |
| Sum of electronic and zero-point energies[e] | −1522.507825 | −1864.121732 | −1409.523823 |
| Sum of electronic and thermal energies[f] | −1522.478830 | −1864.094072 | −1409.497509 |
| Sum of electronic and thermal enthalpies[g] | −1522.477886 | −1864.093128 | −1409.496565 |
| Sum of electronic and thermal free energies[h] | −1522.569904 | −1864.182594 | −1409.582218 |
| E (Thermal)[i] | 294.035 | 264.855 | 270.846 |
| CV[j] | 109.323 | 104.085 | 100.028 |
| S[k] | 193.668 | 188.297 | 180.271 |

[a-h]Hartree/particle; [i]KCal/Mol; [j,k]Cal/Mol-Kelvin.

Starting from the above note, if we plot all MEP surfaces with all isosurface values, we see only the top surface. It is observed from the MEP map in Figure 2 that the nitrogen-bonded oxygen atoms in the $NO_2$ group and the oxygen atoms in the carbonyl groups (C=O) of the rings are negative regions in all compounds because in the resonance form of the nitro group, the oxygen atoms have a negative charge and the nitrogen atom has a positive charge, and in the resonance form of the carbonyl groups, the oxygen atoms have a negative charge and the carbon atom has a positive charge. Thus, oxygen atoms are sites for electrophilic activity. The nitrogen atoms in the ring, which are attached to carbonyl lethal electron groups, are also positively charged; therefore, nitrogen atoms are sites for nucleophilic attraction. As such, these sites provide information about the regions where the compounds can have strong intermolecular interactions.

## 4. Conclusion

In the present study, the three-component reaction between 3-nitrophthalic anhydride, hydrazine monohydrate, dimedone, and aromatic aldehydes in the presence of a novel catalytic amount of $ZrO(NO_3)_2.2H_2O$ to produce 1*H*-indazolo[1,2-*b*]phthalazine-1,6,11(13*H*)-trione derivatives was reported. The reported method offers a mild and efficient procedure for the preparation of these compounds. These compounds of the products were confirmed by IR, $^1$H NMR, $^{13}$C NMR, mass spectra, and elemental analyses. The IR spectra data and $^1$H NMR and $^{13}$C NMR chemical shift computations of the 1*H*-indazolo[1,2-*b*] phthalazine-1,6,11(13*H*)-trione derivatives in the ground state were calculated. There was an excellent agreement between experimental and theoretical results. Frontier molecular orbitals (FMOs), total density of states (DOS), and molecular electrostatic potential (MEP) of the title compounds were investigated through theoretical calculations.

## Data Availability

No data were used to support this study.

## Conflicts of Interest

The authors declare that they have no conflicts of interest.

## Acknowledgments

The authors are thankful to the Zanjan Branch, Islamic Azad University, for partial support of this work.

## Supplementary Materials

Figure S1: 1*H* NMR (62.9 MHz, DMSO) spectrum of 3,3-dimethyl-13-(4-methoxyphenyl)-10-nitro-2,3,4,13-tetrahydro-1*H*-indazolo[1,2-*b*] phthalazine-1,6,11(13*H*)-trione (5a). Figure S2: $^{13}$C NMR (62.9 MHz, DMSO) spectrum of 3,3-dimethyl-13-(4-methoxyphenyl)-10-nitro-2,3,4,13-tetrahydro-1*H*-indazolo[1,2-*b*] phthalazine-1,6,11(13*H*)-trione **(5a).** Figure S3: mass spectrum of 3,3-dimethyl-13-(4-methoxyphenyl)-10-nitro-2,3,4,13-tetrahydro-1*H*-indazolo[1,2-*b*] phthalazine-1,6,11(13*H*)-trione **(5a)**. Figure S4: 1*H* NMR (62.9 MHz, DMSO) spectrum of 3,3-dimethyl-10-nitro-13-phenyl-2,3,4,13-tetrahydro-1*H*-indazolo[1,2-*b*] phthalazine 1,6,11(13*H*)-trione **(5b)**. Figure S5: $^{13}$C NMR (62.9 MHz, DMSO) spectrum of 3,3-dimethyl-10-nitro-13-phenyl-2,3,4,13-tetrahydro-1*H*-indazolo[1,2-*b*] phthalazine-1,6,11(13*H*)-trione **(5b)**. Figure S6: 1*H* NMR (62.9 MHz, DMSO) spectrum of 13-(4-chlorophenyl)-3,3-dimethyl-10-nitro-2,3,4,13-tetrahydro-1*H*-indazolo[1,2-*b*]-phthalazine-

1,6,11(13*H*)-trione **(5c)**. Figure S7: $^{13}$C NMR (62.9 MHz, DMSO) spectrum of 13-(4-chlorophenyl)-3,3-dimethyl-10-nitro-2,3,4,13-tetrahydro-1*H*-indazolo[1,2-*b*]-phthalazine-1,6,11(13*H*)-trione **(5c)** (*Supplementary Materials*)

## References


[1] M. Azab, M. Youssef, and E. El-Bordany, "Synthesis and antibacterial evaluation of novel heterocyclic compounds containing a sulfonamido moiety," *Molecules*, vol. 18, no. 1, pp. 832–844, 2013.

[2] P. Martins, J. Jesus, S. Santos et al., "Heterocyclic anticancer compounds: recent advances and the paradigm shift towards the use of nanomedicine's tool box," *Molecules*, vol. 20, no. 9, pp. 16852–16891, 2015.

[3] F. W. Lichtenthaler, "Unsaturated *O*- and *N*-heterocycles from carbohydrate feedstocks," *Accounts of Chemical Research*, vol. 35, no. 9, pp. 728–737, 2002.

[4] S. Grasso, G. De Sarro, A. De Sarro et al., "Synthesis and anticonvulsant activity of novel and potent 6,7-methylenedioxyphthalazin-1(2H)-ones," *Journal of Medicinal Chemistry*, vol. 43, no. 15, pp. 2851–2859, 2000.

[5] N. Watanabe, Y. Kabasawa, Y. Takase et al., "4-Benzylamino-1-chloro-6-substituted phthalazines: synthesis and inhibitory activity toward phosphodiesterase 5," *Journal of Medicinal Chemistry*, vol. 41, no. 18, pp. 3367–3372, 1998.

[6] Y. Nomoto, H. Obase, H. Takai, M. Teranishi, J. Nakamura, and K. Kubo, "Studies on cardiotonic agents. II. Synthesis of novel phthalazine and 1,2,3-benzotriazine derivatives," *Chemical & Pharmaceutical Bulletin*, vol. 38, no. 8, pp. 2179–2183, 1990.

[7] J. S. Kim, H.-K. Rhee, H. J. Park, S. K. Lee, C.-O. Lee, and H.-Y. Park Choo, "Synthesis of 1-2-substituted-[1,2,3]triazolo [4,5-g]phthalazine-4,9-diones and evaluation of their cytotoxicity and topoisomerase II inhibition," *Bioorganic & Medicinal Chemistry*, vol. 16, no. 8, pp. 4545–4550, 2008.

[8] S. El-Shakka, A. Soliman, and A. Imam, "Synthesis, antimicrobial activity and electron impact of mass spectra of phthalazine-1,4-dione derivatives," *Afinidad*, vol. 66, no. 544, pp. 167–172, 2009.

[9] L. Zhang, L.-P. Guan, X.-Y. Sun, C.-X. Wei, K.-Y. Chai, and Z.-S. Quan, "Synthesis and anticonvulsant activity of 6-Alkoxy-[1,2,4]Triazolo[3,4-a]Phthalazines," *Chemical Biology & Drug Design*, vol. 73, no. 3, pp. 313–319, 2009.

[10] C.-K. Ryu, R.-E. Park, M.-Y. Ma, and J.-H. Nho, "Synthesis and antifungal activity of 6-arylamino-phthalazine-5,8-diones and 6,7-bis(arylthio)-phthalazine-5,8-diones," *Bioorganic & Medicinal Chemistry Letters*, vol. 17, no. 9, pp. 2577–2580, 2007.

[11] J. Li, Y.-F. Zhao, X.-Y. Yuan, J.-X. Xu, and P. Gong, "Synthesis and anticancer activities of novel 1,4-disubstituted phthalazines," *Molecules*, vol. 11, no. 7, pp. 574–582, 2006.

[12] J. Sinkkonen, V. Ovcharenko, K. N. Zelenin et al., "$^{1}$H and $^{13}$C NMR study of 1-Hydrazino-2,3-dihydro-1H-pyrazolo[1,2-a] pyridazine-5,8-diones and -1H-pyrazolo[1,2-b]phthalazine-5,10-diones and their ring-chain tautomerism," *European Journal of Organic Chemistry*, vol. 13, pp. 2046–2053, 2002.

[13] H. R. Shaterian, F. Khorami, A. Amirzadeh, R. Doostmohammadi, and M. Ghashang, "Preparation of heterocyclic containing phthalazine skeleton: 2H Indazolo [2, 1-b] phthalazine-1, 6, 11 ($^{13}$H)-triones," *Journal of the Iranian Chemical Research*, vol. 2, no. 1, pp. 57–62, 2009.

[14] M. Shekouhy and A. Hasaninejad, "Ultrasound-promoted catalyst-free one-pot four component synthesis of 2H-indazolo[2,1-b]phthalazine-triones in neutral ionic liquid 1-butyl-3-methylimidazolium bromide," *Ultrasonics Sonochemistry*, vol. 19, no. 2, pp. 307–313, 2012.

[15] M. Sayyafi, M. Seyyedhamzeh, H. R. Khavasi, and A. Bazgir, "One-pot, three-component route to 2H-indazolo[2,1-b] phthalazine-triones," *Tetrahedron*, vol. 64, no. 10, pp. 2375–2378, 2008.

[16] H. R. Shaterian, M. Ghashang, and M. Feyzi, "Silica sulfuric acid as an efficient catalyst for the preparation of 2H-indazolo [2,1-b]phthalazine-triones," *Applied Catalysis A: General*, vol. 345, no. 2, pp. 128–133, 2008.

[17] H. R. Shaterian, A. Hosseinian, and M. Ghashang, "Reusable silica supported poly phosphoric acid catalyzed three-component synthesis of 2H-indazolo[2,1-b]phthalazine- trione derivatives," *Arkivoc*, vol. 2009, no. 2, pp. 59–67, 2009.

[18] J. M. Khurana and D. Magoo, "Efficient one-pot syntheses of 2*H*-indazolo[2,1-*b*]phthalazine-triones by catalytic $H_2SO_4$ in water–ethanol or ionic liquid," *Tetrahedron Letters*, vol. 50, no. 52, pp. 7300–7303, 2009.

[19] E. Mosaddegh and A. Hassankhani, "A rapid, one-pot, four-component route to 2H-indazolo[2,1-b]phthalazine-triones," *Tetrahedron Letters*, vol. 52, no. 4, pp. 488–490, 2011.

[20] H. R. Shaterian and F. Rigi, "Starch sulfate as an efficient and biodegradable polymer catalyst for one-pot, four-component reaction of 2H-indazolo[2,1-b]phthalazine-triones," *Starch-Stärke*, vol. 63, no. 6, pp. 340–346, 2011.

[21] A. Ramazani, Y. Ahmadi, M. Rouhani, N. Shajari, and A. Souldozi, "The reaction of (*N*-isocyanimino) triphenylphosphorane with an electron-poor *α*-haloketone in the presence of aromatic carboxylic acids: a novel three-component reaction for the synthesis of disubstituted 1,3,4-oxadiazole derivatives," *Heteroatom Chemistry*, vol. 21, no. 6, pp. 368–372, 2010.

[22] A. Ramazani, N. Shajari, A. Mahyari, and Y. Ahmadi, "A novel four-component reaction for the synthesis of disubstituted 1,3,4-oxadiazole derivatives," *Molecular Diversity*, vol. 15, no. 2, pp. 521–527, 2011.

[23] N. Shajari, R. Kazemizadeh, and A. Ramazani, "Efficient one-pot, four-component synthesis of *N*,*N*-dibenzyl-*N*-{1-[5-(3-aryl)-1,3,4-oxadiazol-2-yl]cyclobutyl}amine derivatives from the reaction of (isocyanoimino)triphenylphosphorane, dibenzylamine, an aromatic carboxylic acid and cyclobutanone," *Journal of the Serbian Chemical Society*, vol. 77, no. 9, pp. 1175–1180, 2012.

[24] N. Shajari, R. Ghiasi, and A. Ramazani, "One-pot synthesis of 2-acylaminobenzimidazoles from the reaction between trichloroacetyl isocyanate and 1,2-phenylenediamine derivatives and theoretical study of structure and properties of synthesized 2-acylaminobenzimidazoles," *Journal of the Chilean Chemical Society*, vol. 63, no. 2, pp. 3968–3973, 2018.

[25] R. B. Nazarski, "Physical imageversusstructure relation. Part 14-an attempt to rationalize some acidic region $^{13}$C NMR-pH titration shifts for tetraaza macrocycles throughout the conformational GIAO DFT computational results: a pendant-armcyclamcase," *Journal of Physical Organic Chemistry*, vol. 22, no. 9, pp. 834–844, 2009.

[26] S. Dixit, M. Patil, and N. Agarwal, "Ferrocene catalysed heteroarylation of BODIPy and reaction mechanism studies by EPR and DFT methods," *RSC Advances*, vol. 6, no. 53, pp. 47491–47497, 2016.

[27] L. Zheng, Y. Qiao, M. Lu, and J. Chang, "Theoretical investigations of the reaction between 1,4-dithiane-2,5-diol and azomethine imines: mechanisms and diastereoselectivity,"

*Organic & Biomolecular Chemistry*, vol. 13, no. 27, pp. 7558–7569, 2015.

[28] A. Bekhradnia and P.-O. Norrby, "New insights into the mechanism of iron-catalyzed cross-coupling reactions," *Dalton Transactions*, vol. 44, no. 9, pp. 3959–3962, 2015.

[29] D. Duca, G. La Manna, and M. Rosa Russo, "Computational studies on surface reaction mechanisms: ethylene hydrogenation on platinum catalysts," *Physical Chemistry Chemical Physics*, vol. 1, no. 6, pp. 1375–1382, 1999.

[30] S. G. Smith and J. M. Goodman, "Assigning stereochemistry to single diastereoisomers by GIAO NMR calculation: the DP4 probability," *Journal of the American Chemical Society*, vol. 132, no. 37, pp. 12946–12959, 2010.

[31] Z. Yang, P. Yu, and K. N. Houk, "Molecular dynamics of dimethyldioxirane C-H oxidation," *Journal of the American Chemical Society*, vol. 138, no. 12, pp. 4237–4242, 2016.

[32] P. E. Hansen and J. Spanget-Larsen, "Structural studies on Mannich bases of 2-Hydroxy-3,4,5,6-tetrachlorobenzene. An UV, IR, NMR and DFT study. A mini-review," *Journal of Molecular Structure*, vol. 1119, pp. 235–239, 2016.

[33] S. Demir, A. O. Sarioğlu, S. Güler, N. Dege, and M. Sönmez, "Synthesis, crystal structure analysis, spectral IR, NMR UV-Vis investigations, NBO and NLO of 2-benzoyl-*N*-(4-chlorophenyl)-3-oxo-3-phenylpropanamide with use of X-ray diffractions studies along with DFT calculations," *Journal of Molecular Structure*, vol. 1118, pp. 316–324, 2016.

[34] S. K. Saha, A. Hens, N. C. Murmu, and P. Banerjee, "A comparative density functional theory and molecular dynamics simulation studies of the corrosion inhibitory action of two novel *N*-heterocyclic organic compounds along with a few others over steel surface," *Journal of Molecular Liquids*, vol. 215, pp. 486–495, 2016.

[35] G. M. Anderson, I. Cameron, and J. A. Murphy, "Predicting the reducing power of organic super electron donors," *RSC Advances*, vol. 6, no. 14, pp. 11335–11343, 2016.

[36] J. L. Tuttle and S. D. Wetmore, "Selecting DFT methods for use in optimizations of enzyme active sites: applications to ONIOM treatments of DNA glycosylases," *Canadian Journal of Chemistry*, vol. 91, no. 7, pp. 559–572, 2013.

[37] A. D. Becke, "Density-functional thermochemistry. III. The role of exact exchange," *The Journal of Chemical Physics*, vol. 98, no. 7, pp. 5648–5652, 1993.

[38] M. J. Frisch, G. W. Trucks, and H. B. Schlegel, *Gaussian 03, Revision B03*, Gaussian Inc., Pittsburgh, PA, USA, 2003.

[39] L. Shiri, D. Sheikh, A. Faraji, M. Sheikhi, and S. Katouli, "Selective oxidation of oximes to their corresponding carbonyl compounds by sym-collidinium chlorochromate (S-COCC) as a efficient and novel oxidizing agent and theoretical study of NMR shielding tensors and thermochemical parameters," *Letters in Organic Chemistry*, vol. 11, no. 1, pp. 18–28, 2014.

[40] A. Soltani, M. T. Baei, M. Mirarab, M. Sheikhi, and E. Tazikeh Lemeski, "The electronic and structural properties of BN and BP nano-cages interacting with OCN−: a DFT study," *Journal of Physics and Chemistry of Solids*, vol. 75, no. 10, pp. 1099–1105, 2014.

[41] A. Frisch, A. B. Nielson, and A. J. Holder, *GAUSSVIEW User Manual*, Gaussian Inc., Pittsburgh, PA, USA, 2000.

[42] S. Guidara, H. Feki, and Y. Abid, "Molecular structure, NLO, MEP, NBO analysis and spectroscopic characterization of 2,5-dimethylanilinium dihydrogen phosphate with experimental (FT-IR and FT-Raman) techniques and DFT calculations," *Spectrochimica Acta Part A: Molecular and Biomolecular Spectroscopy*, vol. 133, pp. 856–866, 2014.

[43] H. Yahyaei, A. R. Kazemizadeh, and A. Ramazani, "Synthesis and chemical shifts calculation of α-Acyloxycarboxamides derived from indane-1,2,3-trione by DFT and HF methods," *Chinese Journal of Structural Chemistry*, vol. 31, pp. 1346–1356, 2012.

[44] K. G. Vipin Das, C. Yohannan Panicker, B. Narayana, P. S. Nayak, and B. K. Sarojini, "FT-IR, molecular structure, first order hyperpolarizability, NBO analysis, HOMO and LUMO and MEP analysis of 1-(10H-phenothiazin-2-yl) ethanone by HF and density functional methods," *Spectrochimica Acta Part A: Molecular and Biomolecular Spectroscopy*, vol. 135, pp. 162–171, 2015.

[45] S. Al-Saadi and N. Sundaraganesan, "The spectroscopic (FT-IR, FT-IR gas phase, FT-Raman and UV) and NBO analysis of 4-Hydroxypiperidine by density functional method," *Spectrochimica Acta Part A: Molecular and Biomolecular Spectroscopy*, vol. 75, no. 3, pp. 941–952, 2010.

[46] T. Koopmans, "Über die Zuordnung von Wellenfunktionen und Eigenwerten zu den Einzelnen Elektronen Eines Atoms," *Physica*, vol. 1, no. 1-6, pp. 104–113, 1934.

[47] A. Soltani, F. Ghari, A. D. Khalaji et al., "Crystal structure, spectroscopic and theoretical studies on two Schiff base compounds of 2,6-dichlorobenzylidene-2,4-dichloroaniline and 2,4-dichlorobenzylidene-2,4-dichloroaniline," *Spectrochimica Acta Part A: Molecular and Biomolecular Spectroscopy*, vol. 139, pp. 271–278, 2015.

[48] R. G. Pearson, "Chemical hardness and density functional theory," *Journal of Chemical Sciences*, vol. 117, no. 5, pp. 369–377, 2005.

[49] F. J. Luque, J. M. López, and M. Orozco, "Perspective on "Electrostatic interactions of a solute with a continuum. A direct utilization of ab initio molecular potentials for the prevision of solvent effects," *Theoretical Chemistry Accounts*, vol. 103, pp. 343–345, 2000.

[50] K. Chandrasekaran and R. Thilak Kumar, "Structural, spectral, thermodynamical, NLO, HOMO, LUMO and NBO analysis of fluconazole," *Spectrochimica Acta Part A: Molecular and Biomolecular Spectroscopy*, vol. 150, pp. 974–991, 2015.